Article

Not peer-reviewed version

Surface Thermodynamic Properties of 3D/4D Printing Poly Lactic Acid by Inverse Gas Chromatography

Tayssir Hamieh *

Posted Date: 4 March 2024

doi: 10.20944/preprints202403.0176.v1

Keywords: 3D/4D printing; adhesion; London and polar surface energies; glass transition; enthalpic and entropic Lewis's acid–base constants; acid and base surface energies

Article

Surface Thermodynamic Properties of 3D/4D Printing Poly Lactic Acid by Inverse Gas Chromatography

Tayssir Hamieh [1,2]

[1] Faculty of Science and Engineering, Maastricht University, P.O. Box 616, 6200 MD Maastricht, The Netherlands; t.hamieh@maastrichtuniversity.nl; Tel.: +31-6-5723-9324

[2] Laboratory of Materials, Catalysis, Environment and Analytical Methods (MCEMA), Faculty of Sciences, Lebanese University, Hadath P.O. Box 6573, Lebanon

Abstract: The poly lactic acid (PLA) is one of the most used bio-derived thermoplastic polymers in 3D and 4D printing applications. The determination of PLA surface properties is of capital importance in 3D/4D printing technology. (1) Background: The surface thermodynamic properties of PLA polymer were determined by using the inverse gas chromatography (IGC) technique at infinite dilution. The determination of the retention volume of polar and non-polar molecules adsorbed on the PLA particles filling the column allowed us to obtain the dispersive, polar, and Lewis's acid-base surface properties at different temperatures from 40 °C to 100 °C. (2) Methods: the applied surface method was based on our recent model that used the London dispersion equation and the new chromatographic parameter function of the deformation polarizability and the harmonic mean of the ionization energies of the PLA polymer and organic molecules. (3) Results: The application of this new method led to the determination of the dispersive and polar free surface energy of adsorption of molecules on the polymeric material, as well as the glass transition and the Lewis acid-base constants. (4) Conclusions: four interval temperatures were distinguished showing four zones of the variations of the surface properties of PLA as a function of the temperature before and after the glass transition.

Keywords: 3D/4D printing; adhesion; London and polar surface energies; glass transition; enthalpic and entropic Lewis's acid–base constants; acid and base surface energies

1. Introduction

Since the first description of three-dimensional (3D) printing in the 1980s, many publications were devoted to the additive manufacturing, also known as 3D printing, which was extremely developed in many applications such as engineering, materials science, physics and astronomy, computer science, chemistry, mathematics, genetics, and molecular biology, varying from biomedical engineering, and precision manufacturing to the aerospace and military industries [1–10]. In 3D printing, the three-dimensional object is created from a digital model by adding material, typically in successive layers, on the contrary of traditional manufacturing technologies such as machining, grinding, and casting, where molten material is filled in a mold to create a product [1–4]. Seven classes were distinguished in 3D printing technologies: material extrusion, material jetting, binder jetting, powder bed fusion, directed energy deposition, sheet lamination, and vat photopolymerization [1].

The increasing evolution of the spatial technology of 3D printing led to the fourth-dimensional printing (4D printing) by considering the fourth dimension of time to modulate one or more properties of the 3D printed objects with the help of smart materials that can control the application of any external stimulus implying light, water, self-diagnostic, heating, pressure, and shape-changing effects [1–4,11–16].

Preprints.org (www.preprints.org) | NOT PEER-REVIEWED | Posted: 4 March 2024 doi:10.20944/preprints202403.0176.v1

One of the most used materials in 3D/4D printing is the poly (lactic acid) (PLA), because of its unique properties such as good appearance, higher transparency, less toxicity, and low thermal expansion that help reduce the internal stresses caused during cooling [17–21]. The PLA, a bio-derived thermoplastic polymer, is a 100% biodegradable polymer with high tensile strength and modulus and easily synthesized from lactic acid obtained from corn, sugarcane, and other biomass. It can be recycled up to 8 times and is compostable at the end of life [1,22].

The highest tensile and flexural strengths of PLA and the use of its composites with bio-derived reinforcements such as flax, hemp, jute, bamboo, and other natural fibres were widely researched for 3D printing to enhance mechanical properties, reduce material and production cost, and improve the sustainability of manufactured products [1,22–34].

PLA, a biodegradable aliphatic polyester, is produced from renewal resources has received much attention in the research of alternative biodegradable polymers [35–37]. This PLA polymer is the most popular polymer in the world and may be processed using standard machines, equipment and technologies for classic polymers [35,38,39]. PLA shows good biocompatibility and physical properties, such as high mechanical strength, thermoplasticity and fabricability [35].

The biodegradable PLA polymer is the most used material worldwide for 3D printing [1,22,23,35], and very solicited in 4D printing technology. PLA is an excellent bio-derived polymer is now used as a shape-memory polymer in 4D printing applications [28–33]. The future of 4D printing biocomposites involves multi-disciplinary research to combine design strategies, material properties, stimulus properties, and composite mechanics [1].

The surface properties, the Lewis acid-base parameters, and the dispersive and polar energies of PLA polymer are very important to be determined in many 3D and 4D applications involving the mechanical, adhesion and surface properties. Such properties were not correctly determined in literature.

In this paper, we were interested in determining the surface thermodynamic properties and the various variables of interactions between PLA polymer and other organic molecules. The technique used to study the polymer material was the inverse gas chromatography (IGC) technique at infinite dilution (ID). Our new models [40–46] were applied to quantify the dispersive and polar interaction energies to understand the behavior of PLA polymer and, therefore, to predict the various superficial thermodynamic properties of this 3D/4D printing material in interaction with organic molecules.

The London dispersive interaction [47] between the solvents and the solid materials was determined by applying the London equation and the notion of polarizabilities and ionization energies of the organic molecules and the polymeric material. This new methodology led to the separation between the dispersive and polar surface free energies of PLA and to the accurate determination of the Lewis enthalpic and entropic acid–base constants, the polar acid and base surface energies, and the glass transition of the PLA polymer.

2. Methods and Materials

In this paper, the inverse gas chromatography (IGC) at infinite dilution (ID) was used to determine the net retention time of organic solvents adsorbed on the solid material [48–60]. This results in the calculation of the net retention volume Vn of the adsorbed probes, and therefore to the values of the free energy of adsorption ΔG_a^0 of organic molecules adsorbed on PLA polymer given by the following equation:

$$\Delta G_a^0(T) = -RTlnVn + K(T) \tag{1}$$

Where T is the absolute temperature, R the perfect constant gas and $K(T)$ a constant depending on the temperature and the interaction solvents-PLA

$\Delta G_a^0(T)$ is expressed at any temperature by the summation of the London dispersive energy $\Delta G_a^d(T)$ and the polar energy $\Delta G_a^{sp}(T)$:

$$\Delta G_a^0(T) = \Delta G_a^d(T) + \Delta G_a^p(T) \tag{2}$$

Preprints.org (www.preprints.org) | NOT PEER-REVIEWED | Posted: 4 March 2024 doi:10.20944/preprints202403.0176.v1

Many methods and molecular models were used in literature [48–57,61] to separate the two dispersive and polar contributions of the free energy of adsorption. It was previously showed [40–42] that the best method that gave the accurate separation between $\Delta G_a^d(T)$ and $\Delta G_a^p(T)$ was that based on the London dispersion interaction energy given by equation (3):

$$\Delta G_a^d(T) = -\frac{\alpha_{0S}}{H^6}\left[\frac{3\mathcal{N}}{2(4\pi\varepsilon_0)^2}\left(\frac{\varepsilon_S\,\varepsilon_X}{(\varepsilon_S+\ \varepsilon_X)}\alpha_{0X}\right)\right] \tag{3}$$

Where $\mathcal{N}$ is the Avogadro number, ε_0 the dielectric constant of vacuum, α_{0S} and α_{0X} the respective deformation polarizabilities of the solid material denoted by S and the organic molecule denoted by X, separated by a distance H, and ε_S and ε_X their corresponding ionization energies.
By combining equations (1) to (3), equation (4) was obtained:

$$RTlnVn = \frac{\alpha_{0S}}{H^6}\left[\frac{3\mathcal{N}}{2(4\pi\varepsilon_0)^2}\left(\frac{\varepsilon_S\,\varepsilon_X}{(\varepsilon_S+\ \varepsilon_X)}\alpha_{0X}\right)\right] - \Delta G_a^{sp}(T) + K(T) \tag{4}$$

The chosen interaction parameter $\mathcal{P}_{SX}$ was given by equation (5):

$$\mathcal{P}_{SX} = \frac{\varepsilon_S\,\varepsilon_X}{(\varepsilon_S+\ \varepsilon_X)}\alpha_{0X} \tag{5}$$

For non-polar molecules such as n-alkanes, the representation of $RTlnVn$ of as a function of $\left[\frac{3\mathcal{N}}{2(4\pi\varepsilon_0)^2}\left(\frac{\varepsilon_S\,\varepsilon_X}{(\varepsilon_S+\ \varepsilon_X)}\alpha_{0X}\right)\right]$ of adsorbed molecules is given by equation (6):

$$RTlnVn(non-polar) = A\left[\frac{3\mathcal{N}}{2(4\pi\varepsilon_0)^2}\mathcal{P}_{SX}(non-polar)\right] - K(T) \tag{6}$$

where A is the slope of the non-polar straight line given by:

$$A = \frac{\alpha_{0S}}{H^6} \tag{7}$$

For a polar molecule adsorbed on PLA polymer, the geometric point representing the polar probe will be located outside the straight line of n-alkanes and the distance between the polar point and this straight line will be equal to $\Delta G_a^p(polar)$ of the polar molecule, at chosen temperature.

$$\Delta G_a^p(T, polar) = RTlnVn\,(T, polar) - A\left[\frac{3\mathcal{N}}{2(4\pi\varepsilon_0)^2}\mathcal{P}_{SX}(polar)\right] + K(T) \tag{8}$$

In the case of linear variations of $\Delta G_a^p(T)$ of polar probes as a function of the temperature, it is possible to deduce the specific enthalpy $(-\Delta H_a^p)$ and entropy $(-\Delta S_a^p)$ of polar probes adsorbed on PLA polymer by using the classic thermodynamic relation (9)):

$$\Delta G_a^p(T) = \Delta H_a^p - T\Delta S_a^p \tag{9}$$

The determination of $(-\Delta H_a^p)$ and $(-\Delta S_a^p)$ of adsorbed polar molecules leads to characterize the Lewis's acid-base properties of PLA polymer by its enthalpic (K_A, K_D) and entropic (ω_A, ω_D) acid-base constants using the following relations:

$$\begin{cases}(-\Delta H^p) = \ K_A \times DN' + K_D \times AN' \\ (-\Delta S_a^p) = \omega_A\ \times DN' + \omega_D\ \times AN'\end{cases} \tag{10}$$

where $DN'$and $AN'$are, respectively, the corrected electron donor and acceptor numbers of the polar molecule [62,63].

Experimental results showed that the relations (10) were not always satisfied. In similar cases, other relations (11) were proposed in literature [44,46,64] taking into consideration the amphoteric coupling constants K_{CC} and ω_{CC} of solid materials:

$$\begin{cases}(-\Delta H^p) = \ K_A \times DN' + K_D \times AN' - K_{CC} \times AN' \times DN' \\ (-\Delta S_a^p) = \omega_A\ \times DN' + \omega_D\ \times AN' - \omega_{CC} \times AN' \times DN'\end{cases} \tag{11}$$

Relations (11) can be written as:

$$\begin{cases}a_i\,K_A +\ K_D - b_i\,K_{CC} = (c_H)_i \\ a_i\,\omega_A\ +\ \omega_D - b_i\,\omega_{CC} = (c_S)_i\end{cases} \tag{12}$$

 doi:10.20944/preprints202403.0176.v1

Where a_i, b_i, $(c_H)_i$ and $(c_S)_i$, relative to the adsorbed polar molecule denoted by i, are known experimental values given by equations (13), whereas, K_D, K_A, K_{CC}, ω_A, ω_D and ω_{CC} are the unknown quantities of the problem (12)

$$\begin{cases} a_i = \left(\frac{DN'}{AN'}\right)_i \\ b_i = (DN')_i \\ (c_H)_i = \left(\frac{(-\Delta H^p)}{AN'}\right)_i \\ (c_S)_i = \left(\frac{(-\Delta S^p)}{AN'}\right)_i \end{cases} \quad (13)$$

The unique solution of the system (12) can be obtained if the number n of polar solvents satisfies $n \geq 3$, by using the least squares method. The obtained solution $(K_D;\ K_A; K_{CC})$ or $(\omega_D;\ \omega_A;\ \omega_{CC})$ thus minimizing the sum of the squares of the residuals.

Materials

PLA polymer and all organic solvents (highly pure grade (i.e., 99%) were purchased from Sigma-Aldrich. The various non-polar molecules used in this study were n-alkanes (pentane, hexane, heptane, octane, and nonane); acidic: dichloromethane, amphoteric: acetone and toluene; basic solvents: ethyl acetate and tetrahydrofuran (THF). The PLA particles of size between 100 and 250 ◎m, were introduced into a stainless-steel column, which was 30 cm long and had an internal diameter of 5 mm. A mass of 1 g of PLA was used to fill the chromatographic column. The column filled with the sample was conditioned at 120 °C for 12 h to remove any impurities. Helium was used as carrier gas with a flow-rate equal to 25 mL/min. The IGC measurements at infinite dilution were carried out with a DELSI GC 121 FB Chromatograph equipped with a flame ionization detector of high sensitivity. The injector and detector temperatures were maintained at 180 ºC during the experiments. To achieve infinite dilution approach linear condition gas chromatography, 0.1 ◎L of each probe was injected with 1 ◎L Hamilton syringes. In such a way that the interactions between probe molecules can be neglected and only the interactions between the surface of the solid and an isolated probe molecule are important. The column temperatures were 40 to 100 °C, varied in 5 °C steps. Each probe injection was repeated three times, and the average retention time, was used for the calculation of the retention volume. The standard deviation was less than 1% in all measurements.

3. Results

3.1. London Dispersive Component of Surface Energy of PLA

By using the same procedure developed in previous studies [40,41] and by varying the temperature of the chromatographic column containing the PLA particles, IGC technique allowed us to obtain the net retention times of the various solvents adsorbed on the PLA polymer. This led to the net retention volumes of injected probes and therefore the values of $RTlnVn$ of adsorbed organic molecules. The experimental results were given in Table S1 and S2 (Supporting Materials).

The London dispersive component $\gamma_s^d(T)$ of the surface energy of PLA polymer was obtained by applying the Hamieh thermal model [43–45,64,65]. The variation of $\gamma_s^d(T)$ of PLA polymer as a function of the temperature was plotted on Figure 1.

Preprints.org (www.preprints.org) | NOT PEER-REVIEWED | Posted: 4 March 2024 doi:10.20944/preprints202403.0176.v1

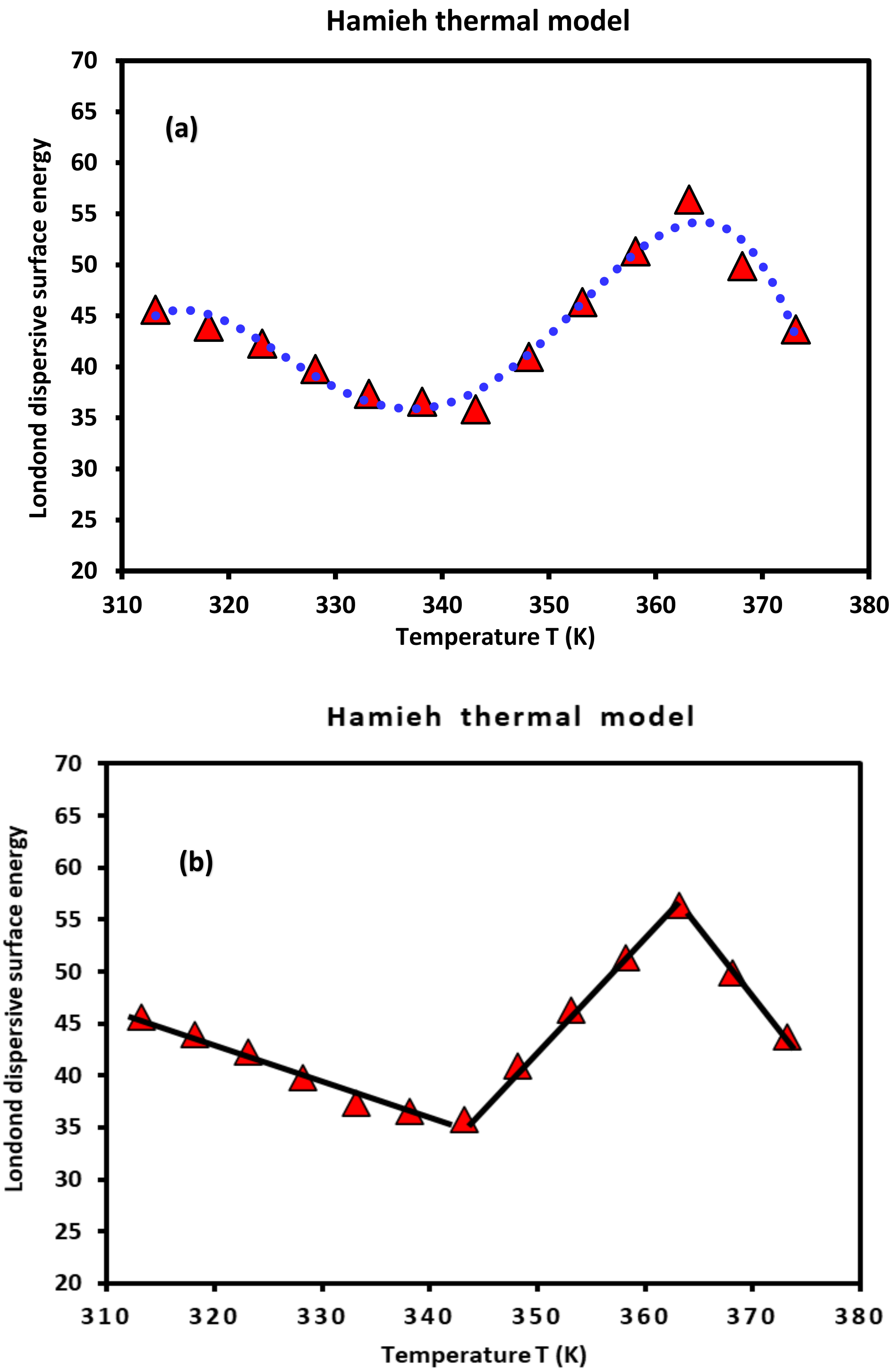

Figure 1. Evolution of γ_s^d (mJ/m^2) of PLA polymer as a function of the temperature T (K) by using the thermal model.

A non-linear evolution of $\gamma_s^d(T)$ was observed (Figure 1a) showing an important change in the thermodynamic properties of PLA when the temperature varies. However, three linear variations were distinguished (Figure 1b) characterized by a decrease of $\gamma_s^d(T)$ in the temperature interval [313.15K, 333.15] given by the equation (14):

$$\gamma_s^d(T) = -0.384\,T + 165.87 \tag{14}$$

Preprints.org (www.preprints.org) | NOT PEER-REVIEWED | Posted: 4 March 2024 doi:10.20944/preprints202403.0176.v1

Passing by a minimum of the London dispersive surface energy equal to 35.8 mJ/m² at $T = 343.15K$, followed by an increase variation of $\gamma_s^d(T$ to reach a maximum equal to 56.4 mJ/m² at $T = 363.15K$, with the following straight-line equation (15):

$$\gamma_s^d(T) = 1.030\,T + 317.68 \tag{15}$$

And finally, a decrease characterized by equation (16):

$$\gamma_s^d(T) = -1.272\,T + 518.31 \tag{16}$$

This interesting result highlighted the possible glass transition temperature of PLA around $T_g = 343.15K$ (70°C) explained by the change in the variations of $\gamma_s^d(T)$ of PLA before and after T_g, when the temperature increases.

3.2. Polar Surface free Energy of PLA polymer

All thermodynamic surface properties of PLA polymer were obtained by using our new method of the harmonic mean of the ionization energies and the deformation polarizability of particles. Tables 1 and 2 respectively presented the values of deformation polarizability, harmonic mean of the ionization energies and the parameter $\mathcal{P}_{PLA-X}$ of the various organic molecules in interaction with the PLA polymer. The Handbook of Physics and Chemistry [66] were used to determine the parameters of the different solvents.

Table 1. Values of deformation polarizability α_0 (respectively in 10^{-30} m³ and in 10^{-40} C m²/V) and ionization energy ε (in eV) of the various organic molecules and PLA polymer.

Molecule	$\boldsymbol{\varepsilon_X}$ **or** $\boldsymbol{\varepsilon_S}$ **(eV)**	$\boldsymbol{\alpha_{0X}}$ **or** $\boldsymbol{\alpha_{0S}}$ **(in 10^{-30} m³)**	$\boldsymbol{\alpha_{0X}}$ **or** $\boldsymbol{\alpha_{0S}}$ **(in 10^{-40} C m²/V)**
n-pentane	10.28	9.99	11.12
n-hexane	10.13	11.90	13.24
n-heptane	9.93	13.61	15.14
n-octane	9.80	15.90	17.69
n-nonane	9.71	17.36	19.32
n-decane	9.65	19.10	21.25
CH_2Cl_2	11.32	7.21	8.02
Tetrahydrofuran	9.38	8.22	9.15
Ethyl acetate	10.01	9.16	10.19
Acetone	9.70	6.37	7.09
Toluene	8.83	11.80	13.13
PLA	14.85	3.35	3.73

Table 2. Values of the harmonic mean of the ionization energies of PLA particles and organic solvents (in 10^{-19} J) and the parameter $\frac{3\mathcal{N}}{2(4\pi\varepsilon_0)^2}\mathcal{P}_{PLA-X}$ (in 10^{-15} SI unit) for the various organic molecules.

Molecule X	$\frac{\varepsilon_{PLA}\,\varepsilon_X}{(\varepsilon_{PLA}+\varepsilon_X)}$ **(in 10^{-19} J)**	$\frac{3\mathcal{N}}{2(4\pi\varepsilon_0)^2}\mathcal{P}_{PLA-X}$ **(in 10^{-15} SI)**
C5	6.075	78.831
C6	6.022	93.088
C7	5.951	105.205
C8	5.904	121.937
C9	5.871	132.395
CH_2Cl_2	6.423	60.160
Ethyl acetate	5.979	71.147
Acetone	5.869	48.559
Toluene	5.536	84.863
THF	5.749	61.383

Preprints.org (www.preprints.org) | NOT PEER-REVIEWED | Posted: 4 March 2024 doi:10.20944/preprints202403.0176.v1

The obtained experimental results (Tables S1 and S2), the values in Tables 1 and 2 and the equations 2, 4, and 8 allowed us to calculate the polar free surface energy ($-\Delta G_a^{sp}(T)$) of the polar solvents adsorbed on PLA polymer as a function of the temperature T (Table 3).

Table 3. Values of $-\Delta G_a^{p}(T)$ (in kJ/mol) of polar molecules adsorbed on PLA.

T(K)	CH_2Cl_2	Ethyl Acetate	Acetone	Toluene	THF
313.15	9.641	3.355	5.097	9.721	8.784
318.15	8.979	2.775	4.875	9.369	8.326
323.15	8.317	2.214	4.634	9.017	7.867
328.15	7.636	1.683	4.321	8.712	7.409
333.15	6.955	1.221	4.230	8.406	6.950
338.15	7.987	3.227	7.213	9.345	9.145
343.15	9.018	5.044	10.980	10.284	11.356
348.15	7.748	4.165	7.543	9.437	8.756
353.15	6.478	2.667	3.675	8.591	5.742
358.15	6.364	2.211	3.054	8.449	5.433
363.15	6.250	1.825	2.654	8.307	5.124
368.15	6.104	1.583	2.305	8.122	4.811
373.15	5.934	1.265	2.005	7.987	4.435

The results in Table 3 showed an amphoteric behavior of PLA with stronger basic character which is clearly shown by the high values of $-\Delta G_a^{sp}(T)$ of dichloromethane, the most acidic solvent among the five used polar molecules, and then traducing the important interaction energy with PLA. It was observed in Table 3 that the variations of $-\Delta G_a^{sp}(T)$ for all polar molecules, are not linear. The curves of $-\Delta G_a^{sp}(T)$ of polar solvents adsorbed on PLA in Figure 2 proved this non-linearity against the temperature with a maximum temperature around 343.15 K confirming the presence of the glass temperature of PLA which was previously shown with the variations of London dispersive surface energy $\gamma_s^d(T)$ as a function of the temperature.

 doi:10.20944/preprints202403.0176.v1

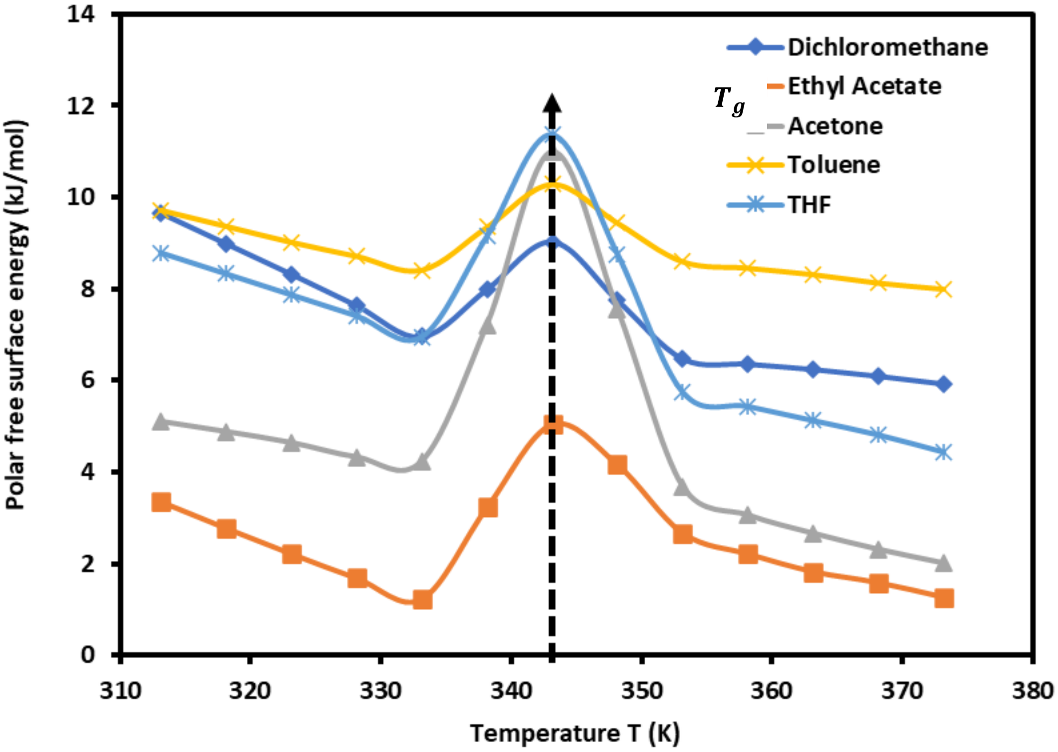

Figure 2. Variations of the polar free surface energy ($-\Delta G_a^{sp}(T)$) of polar solvents adsorbed on PLA polymer as a function of the temperature.

3.3. Lewis's Acid–Base Constants of PLA

The curves of ($-\Delta G_a^{sp}(T)$) of polar molecules drawn in Figure 2 showed four different temperature intervals in which the variations of ($-\Delta G_a^{sp}(T)$) are represented by straight line with an excellent linear regression coefficient equal to 0.9990. The results were given in Table 4 with the different equations.

Table 4. Equations of $-\Delta G_a^{sp}(T)$ of the polar solvents adsorbed on PLA for the different temperature intervals.

Solvent	[313.15K, 333.15K]	[333.15K, 343.15K]	[343.15K, 353.15K]	[353.15K, 373.15K]
CH_2Cl_2	$-\Delta G_a^{sp} = -0.134T + 51.718$	$-\Delta G_a^{sp} = 0.206T - 61.799$	$-\Delta G_a^{sp} = -0.254T + 96.18$	$-\Delta G_a^{sp} = -0.029T + 16.66$
Ethyl Acetate	$-\Delta G_a^{sp} = -0.107T + 36.894$	$-\Delta G_a^{sp} = 0.383T - 126.11$	$-\Delta G_a^{sp} = -0.238T + 86.728$	$-\Delta G_a^{sp} = -0.062T + 24.245$
Acetone	$-\Delta G_a^{sp} = -0.046T + 19.418$	$-\Delta G_a^{sp} = 0.675T - 220.79$	$-\Delta G_a^{sp} = -0.731T + 261.73$	$-\Delta G_a^{sp} = -0.070T + 28.074$
Toluene	$-\Delta G_a^{sp} = -0.066T + 30.294$	$-\Delta G_a^{sp} = 0.188T - 54.185$	$-\Delta G_a^{sp} = -0.169T + 68.411$	$-\Delta G_a^{sp} = -0.031T + 19.708$
THF	$-\Delta G_a^{sp} = -0.092T + 37.500$	$-\Delta G_a^{sp} = 0.441T - 139.83$	$-\Delta G_a^{sp} = -0.561T + 204.07$	$-\Delta G_a^{sp} = -0.065T + 28.611$

The values of the polar enthalpy ($-\Delta H_a^p$) and entropy ($-\Delta S_a^p$) of the polar molecules adsorbed on PLA polymer were deduced from the equations of $\Delta G_a^{sp}(T)$ in Table 4. The values of these polar thermodynamic parameters were given in Table 5.

 doi:10.20944/preprints202403.0176.v1

Table 5. Values of polar enthalpy ($-\Delta H_a^p$ *in* kJ mol^{-1}) and entropy ($-\Delta S_a^p$ *in* J K^{-1}mol^{-1}) of polar probes adsorbed on PLA.

Polar enthalpy ($-\Delta H_a^p$ *in* kJ mol^{-1})				
Solvent	[313.15K, 333.15K]	[333.15K, 343.15K]	[343.15K, 353.15K]	[353.15K, 373.15K]
CH_2Cl_2	51.718	-61.799	96.177	16.661
Ethyl Acetate	36.894	-126.11	86.728	24.245
Acetone	19.418	-220.79	261.73	28.074
Toluene	30.294	-54.185	68.411	19.708
THF	37.5	-139.83	204.07	28.611
Polar entropy ($-\Delta S_a^p$ *in* J K^{-1}mol^{-1})				
Solvent	[313.15K, 333.15K]	[333.15K, 343.15K]	[343.15K, 353.15K]	[353.15K, 373.15K]
CH_2Cl_2	134.3	-206.4	254	28.7
Ethyl Acetate	107.2	-382.3	237.7	61.6
Acetone	45.8	-675	730.5	69.9
Toluene	65.8	-187.9	169.4	31.4
THF	91.7	-440.6	561.4	64.7

Table 5 allowed us to draw on Figure 3 the curves of ($-\Delta H_a^p(T)$) and entropy ($-\Delta S_a^p$(T)) of polar molecules as a function of the temperature

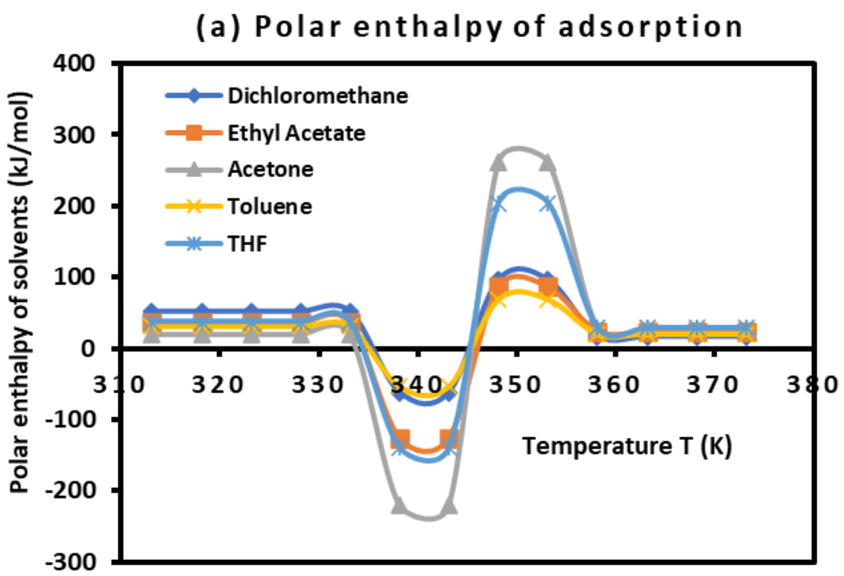

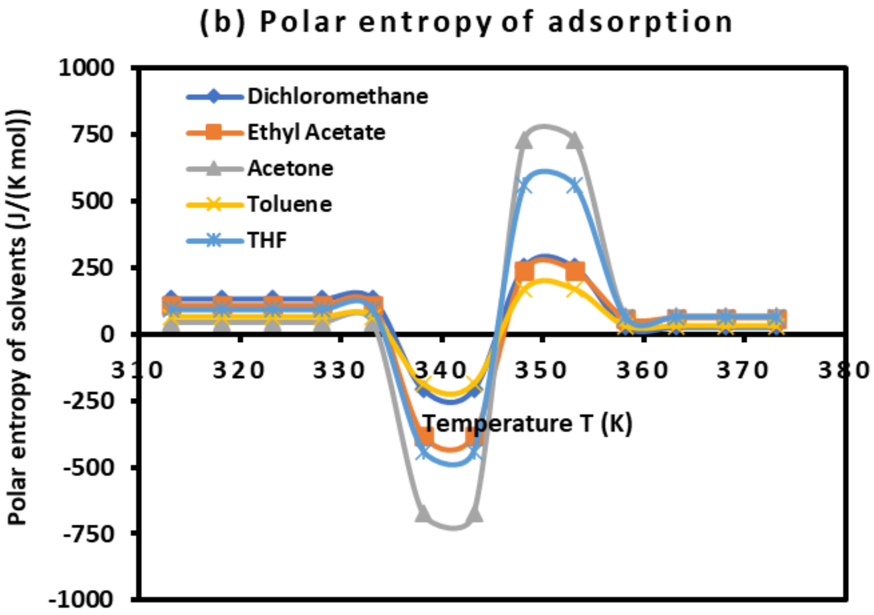

Figure 3. Variations of $(-\Delta H_a^p(T))$ (a) and entropy $(-\Delta S_a^p(\mathrm{T}))$ (b) of polar molecules adsorbed on PLA polymer as a function of the temperature.

It was observed that the curves of Figure 3 present positive values of polar enthalpy and entropy of polar solvents before and after the glass transition temperature highlighting the adsorption phenomenon, whereas, the desorption was observed during the transition process showing a repulsive interaction around the glass transition.

By using the empirical relation (10) and the results in Table 5 and Figure 3, the Lewis enthalpic and entropic acid–base constants K_A, K_D, ω_A, and ω_D of PLA polymer as a function of the temperature with their ratios were given in Table 6.

Table 6. Values of the enthalpic acid–base constants K_A and K_D (unitless), the entropic acid base constants ω_A and ω_D (unitless), the acid–base ratios of PLA, and the linear regression coefficients.

Temperature T (K)	K_A	K_D	K_D/K_A	R^2	$10^3\times \omega_A$	$10^3\times \omega_D$	ω_D / ω_A	R^2
313.15	0.359	1.963	5.47	0.8168	0.89	4.83	5.43	0.8557
318.15	0.359	1.963	5.47	0.8168	0.89	4.83	5.43	0.8557
323.15	0.359	1.963	5.47	0.8168	0.89	4.83	5.43	0.8557
328.15	0.359	1.963	5.47	0.8168	0.89	4.83	5.43	0.8557
333.15	0.359	1.963	5.47	0.8168	0.89	4.83	5.43	0.8557
338.15	-1.503	-4.417	2.94	0.9779	-4.70	-14.34	3.05	0.9754
343.15	-1.503	-4.417	2.94	0.9779	-4.70	-14.34	3.05	0.9754
348.15	2.259	2.534	1.12	0.9335	6.26	5.92	0.95	0.936
353.15	2.259	2.534	1.12	0.9335	6.26	5.92	0.95	0.936
358.15	0.294	1.096	3.73	0.9099	0.70	1.88	2.68	0.9804
363.15	0.294	1.096	3.73	0.9099	0.70	1.88	2.68	0.9804
368.15	0.294	1.096	3.73	0.9099	0.70	1.88	2.68	0.9804
373.15	0.294	1.096	3.73	0.9099	0.70	1.88	2.68	0.9804

The results in Table 6 showed that the behavior of the PLA surface is 5.5 times more basic than acidic for a temperature less than 333.15K (Figure 4). The desorption of the polar solvents in the glass transition process led to a neutral surface of the polymer for $333.15K < T < 343.15K$ characterized by negative values of the Lewis acid-base constants K_A, K_D, ω_A, and ω_D of PLA. After the glass transition temperature, two zones were distinguished (Figure 4):

Preprints.org (www.preprints.org) | NOT PEER-REVIEWED | Posted: 4 March 2024 doi:10.20944/preprints202403.0176.v1

- Stronger amphoteric character of PLA with highest values of the Lewis acid-base constants for $343.15K < T < 353.15K$
- Decreasing amphoteric behavior of PLA surface with lowest values of K_A, K_D, ω_A, and ω_D of the polymer for $T > 353.15K$

Table 6 and Figure 4 clearly showed the stronger basic character of PLA varying with the temperature and decreasing amphoteric behavior for larger temperatures ($T > 353.15K$)

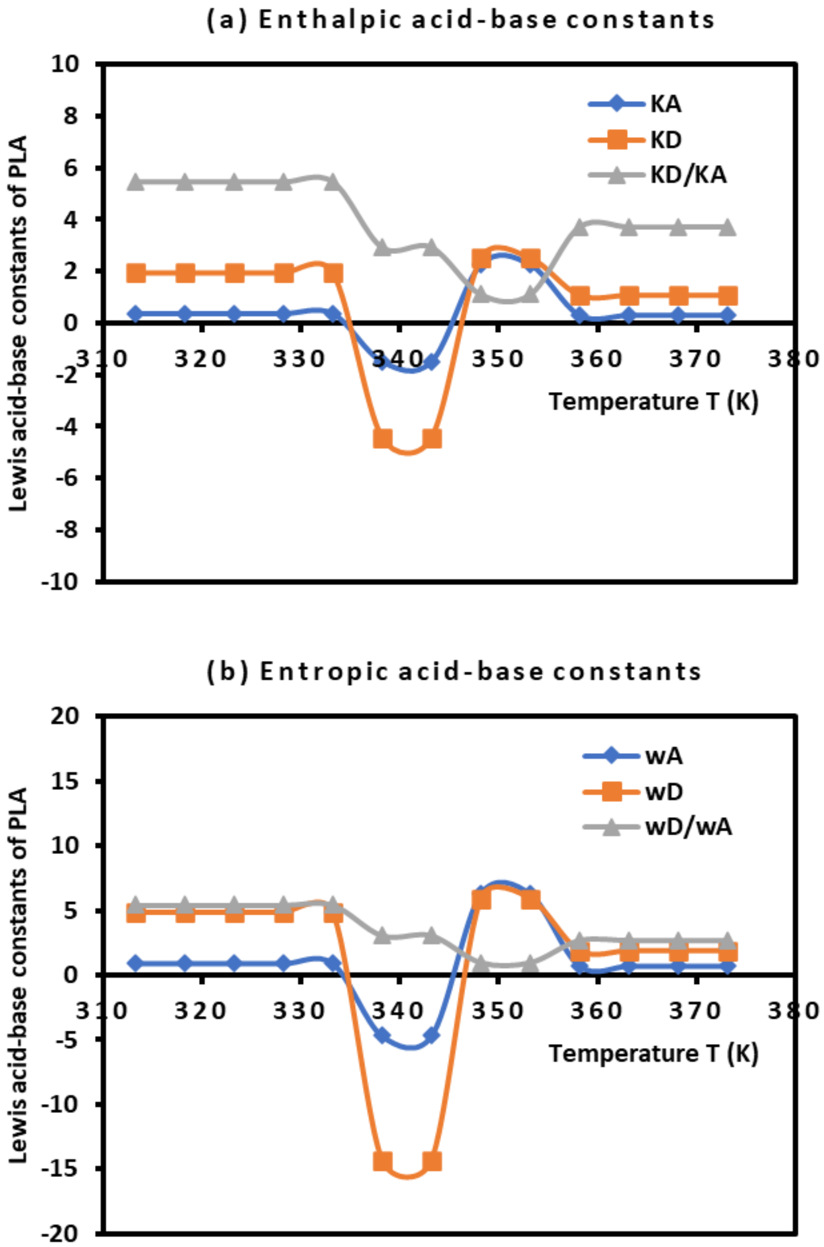

Figure 4. Variations of the Lewis enthalpic acid–base constants K_A and K_D (a) and the Lewis entropic acid base constants ω_A and ω_D (b) as a function of the temperature.

Correction of the acid-base parameters of PLA

The validity of the equations (10) was not always satisfied as was shown by the values of the linear regression coefficients R2 given in Table 6. The correction reported by Hamieh et al. in other papers was applied in this work to give more accurate values of the acid-base constants of PLA polymer. Equations (11) to (13) were used with procedure developed in a recent paper [42]. The corrected results were presented in Table 7.

 doi:10.20944/preprints202403.0176.v1

Table 7. Values of the corrected acid–base constants K_A, K_D, $\boldsymbol{K_{CC}}$, ω_A, ω_D, $\boldsymbol{\omega_{CC}}$ and the acid–base ratios of PLA.

Temperature T (K)	K_A	K_D	$10^2\times K_{CC}$	K_D/K_A	$10^3\times\omega_A$	$10^3\times\omega_D$	$10^5\times\omega_{CC}$	ω_D/ω_A
313.15	0.332	1.651	1.8	4.98	0.83	4.20	3.7	5.03
318.15	0.332	1.651	1.8	4.98	0.83	4.20	3.7	5.03
323.15	0.332	1.651	1.8	4.98	0.83	4.20	3.7	5.03
328.15	0.332	1.651	1.8	4.98	0.83	4.20	3.7	5.03
333.15	0.332	1.651	1.8	4.98	0.83	4.20	3.7	5.03
338.15	-1.503	-4.417	0	2.94	-4.70	-14.34	0	3.05
343.15	-1.503	-4.417	0	2.94	-4.70	-14.34	0	3.05
348.15	2.215	2.040	2.9	0.92	6.16	4.77	0.7	0.77
353.15	2.215	2.040	2.9	0.92	6.16	4.77	0.7	0.77
358.15	0.283	0.972	0.7	3.43	0.69	1.78	0.6	2.58
363.15	0.283	0.972	0.7	3.43	0.69	1.78	0.6	2.58
368.15	0.283	0.972	0.7	3.43	0.69	1.78	0.6	2.58
373.15	0.283	0.972	0.7	3.43	0.69	1.78	0.6	2.58

The comparison between the results in Tables 6 and 7 showed that the error committed by neglecting the amphoteric constant reaches 25%, however, the tendency of the acid-base behavior of PLA remains the same with two used methods.

3.3. Dispersive and Polar Free Energy of PLA

This new method applied on the PLA polymer using the London dispersion interaction equation resulted in the net separation of the London dispersive free energy $\Delta G_a^d(T)$ and the polar free energy $\Delta G_a^p(T)$ of interaction between the PLA and the adsorbed organic molecules. By using equation (3), it was possible to experimentally determine the values of $\Delta G_a^d(T)$ of all molecules adsorbed on the PLA polymer from the following equation:

$$\Delta G_a^d(T) = A\left[\frac{3\mathcal{N}}{2(4\pi\varepsilon_0)^2}\mathcal{P}_{SX}\right] \tag{17}$$

Where the values of the parameter A was determined from the experimental results (Table 8).

Table 8. Values of the parameter A as a function of the temperature.

Temperature T (K)	Parameter $\boldsymbol{A}$ (SI unit)
313.15	5.93×10^{-2}
318.15	5.84×10^{-2}
323.15	5.76×10^{-2}
328.15	5.59×10^{-2}
333.15	5.42×10^{-2}
338.15	5.38×10^{-2}
343.15	5.35×10^{-2}
348.15	5.73×10^{-2}
353.15	6.12×10^{-2}
358.15	6.49×10^{-2}
363.15	6.87×10^{-2}
368.15	6.53×10^{-2}
373.15	6.19×10^{-2}

It was observed that the variations of the parameter A given in Table 7 passed through a minimum corresponding exactly to the glass transition temperature $T_g = 343.15K$.

Preprints.org (www.preprints.org) | NOT PEER-REVIEWED | Posted: 4 March 2024 doi:10.20944/preprints202403.0176.v1

The values of $\Delta G_a^d(T)$ of the adsorbed organic molecules were determined (Tables S3 and S4). The obtained results led drawing the variations of $\Delta G_a^d(T)$ also showed a minimum at glass transition as was shown in Figure 5.

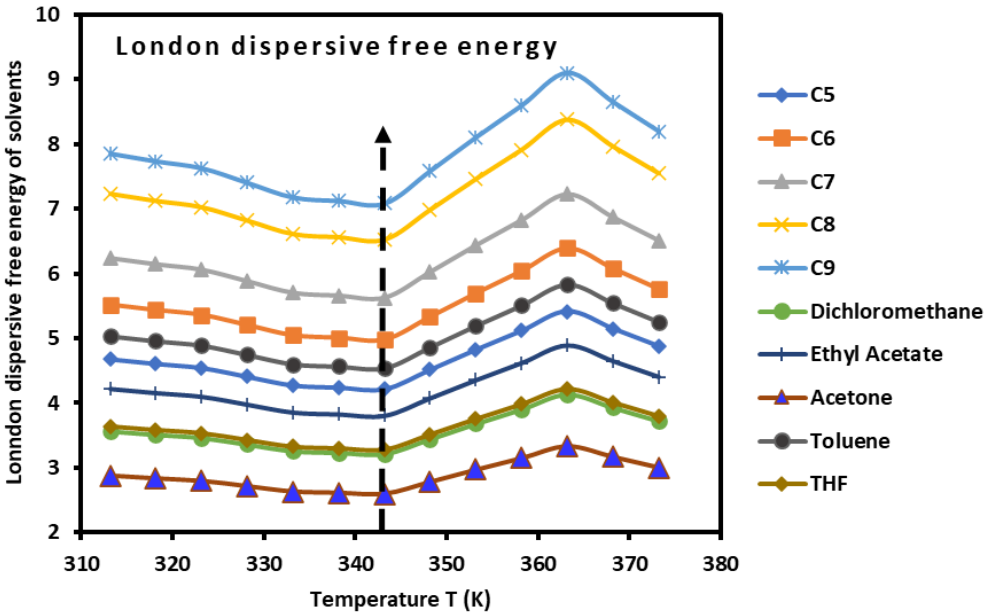

Figure 5. Variations the London dispersive free energy $\Delta G_a^d(T)$ (kJ/mol) of polar molecules adsorbed on PLA polymer as a function of the temperature.

The experimental determination of the dispersive $\Delta G_a^d(T)$ and polar $\Delta G_a^p(T)$ energy of interaction allowed us to obtain the total free energy $\Delta G_a^0(T)$ of organic molecules (Table S5 and Figure S1) that also highlighted the presence of the glass transition

3.4. Average Separation Distance H

Table 8 and equation 7 allowed determining the average separation distance H between PLA surface and the organic molecules as a function of the temperature. The obtained results are given in Table 9. These results showed a slight variation of the separation distance when the temperature varies, but it respects the general tendency observed with the other thermodynamic variables showing a signature at the glass transition temperature reported for $H = 8.30$Å (Figure S2). The results in Table 9 and Figure S2 showed a small increase of the separation distance when the temperature increases until the glass transition $T < 343.15K$, followed by a slight decrease of H after this temperature. This result confirmed that obtained by the stronger acid-base constants of PLA obtained for $T > 343.15K$.

Table 9. Values of the average separation distance H (in Å) as a function of the temperature.

Temperature T (K)	Separation distance H (in Å)
313.15	8.16
318.15	8.18
323.15	8.20
328.15	8.24
333.15	8.29
338.15	8.30
343.15	8.30
348.15	8.21

353.15	8.12
358.15	8.04
363.15	7.97
368.15	8.03
373.15	8.10

3.4. Lewis Acid-Base Surface Energies of PLA

To determine the acid γ_s^+ and base γ_s^- surface energy of PLA polymer, Van Oss's relation was used [67]:

$$-\Delta G_a^p(X - Polar) = 2\mathcal{N}a_X\left(\sqrt{\gamma_{lX}^-\gamma_s^+} + \sqrt{\gamma_{lX}^+\gamma_s^-}\right) \quad (18)$$

Where γ_{lX}^+ and γ_{lX}^- are the respective acid and base surface energy of the polar molecule X adsorbed on PLA surface with a_X the surface area of the adsorbed solvent.

Using the experimental values relative to ethyl acetate (EA) and dichloromethane (CH_2Cl_2) respectively given by $\gamma_{EA}^+ = 0\,, \gamma_{EA}^- = 19.2\ mJ/m^2$ and $\gamma_{CH2Cl2}^+ = 5.2\ mJ/m^2\,, \gamma_{CH2Cl2}^- = 0\,;$ it was possible to determine the values of γ_s^+ and γ_s^- of PLA polymer by using equations (19):

$$\begin{cases} \gamma_s^+ = \dfrac{\left[\Delta G_a^{sp}(T)\ (EA)\right]^2}{4\mathcal{N}^2[a(EA)]^2\gamma_{EA}^-} \\ \gamma_s^- = \dfrac{\left[\Delta G_a^{sp}(T)\ (CH2Cl2)\right]^2}{4\mathcal{N}^2[a(CH2Cl2)]^2\gamma_{CH2Cl2}^+} \end{cases} \quad (19)$$

Whereas, the acid-base (polar) surface energy γ_s^{AB} of PLA was obtained from equation (20):

$$\gamma_s^{AB} = 2\sqrt{\gamma_s^+\gamma_s^-} \quad (20)$$

The results were reported in Table 10 and Figure S3. The variations of the acid and base surface energies versus the temperature showed a decrease of these surface energy parameters and then an increase reaching a maximum at the glass transition temperature, followed by a final decrease until $T = 373.15K$. An important basic surface energy γ_s^- of PLA was observed with smaller acidic surface energy.

Table 10. Values of the polar acid and base surface energies γ_s^+, γ_s^- and γ_s^{AB} (mJ/m²) of PLA as a function of the temperature.

T(K)	γ_s^-	γ_s^+	γ_s^{AB}
313.15	50.59	4.38	29.78
318.15	43.66	2.98	22.83
323.15	37.27	1.89	16.78
328.15	31.26	1.09	11.65
333.15	25.80	0.57	7.66
338.15	33.86	3.95	23.14
343.15	42.96	9.61	40.64
348.15	31.55	6.52	28.69
353.15	21.95	2.66	15.28
358.15	21.08	1.82	12.39
363.15	20.23	1.23	9.99
368.15	19.20	0.92	8.42
373.15	18.06	0.59	6.51

The results in Table 10 with those relative to the dispersive surface energy of PLA previously obtained in this work, led to the determination of the Lifshitz – Van der Waals (LW) surface energy γ_s^{LW} (Table 11) by using equation (21):

$$\gamma_s^{LW} = \gamma_s^d + \gamma_s^{AB} \quad (21)$$

Table 11. Values of the polar acid and base surface energies γ_s^+, γ_s^- and γ_s^{AB} (mJ/m²) of PLA as a function of the temperature.

T(K)	γ_s^d	γ_s^{LW}
313.15	45.59	75.37
318.15	43.93	66.75
323.15	42.28	59.06
328.15	39.78	51.43
333.15	37.36	45.02
338.15	36.60	59.74
343.15	35.83	76.47
348.15	40.97	69.66
353.15	46.33	61.61
358.15	51.33	63.72
363.15	56.41	66.40
368.15	49.86	58.28
373.15	43.69	50.20

3.5. Polar Component of the Surface Energy of Polar Molecules

By using the previous results and the equation (22) relating the polar free energy of polar molecules adsorbed on PLA to the polar components of the surface energy of the PLA polymer γ_s^{p} and the polar organic molecules γ_l^{p}.

$$\begin{cases} -\Delta G_a^p(X) = 2\mathcal{N} a_X \sqrt{\gamma_s^{p} \gamma_l^{p}} \\ or \;\; \gamma_l^{p} = \frac{\left(-\Delta G_a^p(X)\right)^2}{4\mathcal{N}^2 a_X^2 \gamma_s^{p}} \end{cases} \quad (22)$$

γ_l^{p} of polar molecules was directly obtained from equation (22). The results were given in Table 12

Table 12. Values of γ_l^{p} (mJ/m²) of polar molecules adsorbed on PLA.

T(K)	CH_2Cl_2	Ethyl Acetate	Acetone	Toluene	THF
313.15	16.20	1.08	4.53	7.02	8.52
318.15	17.98	0.96	5.38	8.44	9.91
323.15	20.58	0.82	6.58	10.56	11.94
328.15	24.50	0.68	8.19	14.09	15.13
333.15	30.33	0.54	11.87	19.81	20.09
338.15	13.00	1.23	11.37	8.05	11.43
343.15	9.26	1.69	14.92	5.51	9.95
348.15	9.51	1.61	9.92	6.53	8.32
353.15	12.25	1.23	4.40	10.08	6.66
358.15	14.32	1.03	3.72	11.95	7.30
363.15	16.82	0.86	3.47	14.22	7.99

368.15	18.70	0.76	3.08	16.01	8.29
373.15	22.46	0.62	3.00	19.88	9.05

Table 12 showed that among all obtained values of the polar components of the surface energy of polar molecules, the stronger γ_l^{p} values were obtained with the dichloromethane, the highest acidic solvent used in this study, once again proving the highest Lewis basicity of PLA polymer.

4. Conclusion

Inverse gas chromatography (IGC) at infinite dilution was used to determine the surface thermodynamic properties of the biodegradable poly lactic acid considered as the most interesting material that can be used in 3D and printing applications. The new method used was that based on the London dispersion interaction equation. This equation took into account the polarizability and the harmonic mean of the ionization energies PLA polymer and adsorbed organic solvents. The London dispersive energy of PLA material was determined by using the Hamieh thermal model. The free dispersive and polar energies of adsorbed solvents were obtained by using the new parameter $\mathcal{P}_{SX}$ and the net retention volumes of adsorbed probes from chromatographic measurements. The variations of all thermodynamic parameters of interaction of organic molecules adsorbed on PLA highlighted four temperature intervals with linear equations in each interval of temperature. A glass transition temperature of PLA was located at $T_g = 343.15K$. The presence of this transition phenomenon had an important effect on the non-linearity in the domain of temperature containing the glass transition temperature. This conducted to the strong variation of the enthalpic and entropic acid base constants of PLA as a function of the temperature. A stronger basic character of PLA surface was highlighted before and after the glass transition. A slight variation of the average separation distance between the PLA polymer and the solvents.

The determination of the various components γ_s^+, γ_s^-, and γ_s^{AB} of acid–base surface energies of PLA allowed us to calculate the Lifshitz – Van der Waals surface energy γ_s^{LW}. A dominant basic surface character was shown with a highest value of $\gamma_s^-$of PLA. All these surface parameters confirmed the presence of $T_g = 343.15K$ for the poly lactic acid.

The application of this new method allowed a net separation between the polar and dispersive free energy and also the determination of the polar components of the surface energy of polar solvents adsorbed on PLA polymer. These new findings are very useful and can be directly applied to an accurate determination of the dispersive and polar works of adhesion between the PLA surface and other materials.

Supplementary Materials: The following supporting information can be downloaded at the website of this paper posted on Preprints.org. Table S1. Values of $-RTlnVn$ (in kJ/mol) of the various non-polar solvents adsorbed on PLA polymer as a function of the temperature. Table S2. Values of $-RTlnVn$ (in kJ/mol) of the various polar solvents adsorbed on PLA polymer as a function of the temperature. Table S3. Values of $-\Delta G_a^d(T)$ (kJ/mol) of the various non-polar solvents adsorbed on PLA polymer as a function of the temperature. Table S4. Values of $-\Delta G_a^d(T)$ (kJ/mol) of the various polar solvents adsorbed on PLA polymer as a function of the temperature. Table S5. Values of $-\Delta G_a^0(T)$ (kJ/mol) of the various polar solvents adsorbed on PLA polymer as a function of the temperature. Figure S1. Variations the total free energy $\Delta G_a^d(T)$ (kJ/mol) of polar molecules adsorbed on PLA polymer as a function of the temperature. Figure S2. Variations of the average separation distance H (in Å) as a function of the temperature Figure S3. Variations of the polar acid and base surface energies γ_s^+, γ_s^- and γ_s^{AB} (mJ/m²) of PLA as a function of the temperature.

Funding: This research received no external funding.

Institutional Review Board Statement: Not applicable.

Informed Consent Statement: Not applicable.

Data Availability Statement: The data presented in this study are available in article and Supplementary Materials.

Conflicts of Interest: The author declares no conflicts of interest.

References

1. Lakshmi Priya Muthe, Kim Pickering, Christian Gauss, A Review of 3D/4D Printing of Poly-Lactic Acid Composites with Bio-Derived Reinforcements, Composites Part C, Volume 8, 2022, 100271, https://doi.org/10.1016/j.jcomc.2022.100271
2. Y. Zhang, Y. Gao, L. Michelin, L. Josien, L. Vidal, G. Schrodj, A. Simon-Masseron, J. Lalevée, Photopolymerization of ceramic/zeolite reinforced photopolymers: Towards 3D/4D printing and gas adsorption applications, *Eur. Polym. J.* 2022, 179, 111552.
3. J. Yin, X. Zhao, B. Hu, Q. Zhou, Y. Yu, Y. Zhang, J. Gao, Y. Xu, J. Lalevée, Fabrication of a Novel Fluorescein Embedded Photocomposite Based on Interpenetrating Polymer Network (IPN) and Its Application in 4D Printing. *Adv. Mater. Technol.* 2024, 9, 2301323. https://doi.org/10.1002/admt.202301323
4. X. Zheng, H. Lee, T. H. Weisgraber, M. Shusteff, J. Deotte, E. B. Duoss, J. D. Kuntz, M. M. Biener, Q. Ge, J. A. Jackson, S. O. Kucheyev, N. X. Fang, C. M. Spadaccini, Ultraléger, ultra-rigideMétamatériaux mécanique, *Science* 2014, 344, 1373.
5. J. W. Stansbury, M. J. Idacavage, 3D printing with polymers: Challenges among expanding options and opportunities, *Dent. Mater.* 2016, 32, 54-64.
6. M. Shahbazi, H. Jäger, R. Ettelaie, A. Mohammadi, P. Asghartabar Kashi, Multimaterial 3D printing of self-assembling smart thermo-responsive polymers into 4D printed objects: A review, *Addit. Manuf.* 2023, 71, 103598.
7. C. Hull, Apparatus for production of three-dimensional objects by stereothography, United States Patent No. 4575330, 1986.
8. B. Jian, F. Demoly, Y. Zhang, H. J. Qi, J.-C. André, S. Gomes, Origami-Based Design for 4D Printing of 3D Support-Free Hollow Structures, *Engineering* 2022, 12, 70-82.
9. Y. Zhang, Y. Xu, A. Simon-Masseron, J. Lalevée, Radical photoinitiation with LEDs and applications in the 3D printing of composites, *Chem. Soc. Rev.* 2021, 50, 3824.
10. J. J. Schwartz, A. J. Boydston, Multimaterial actinic spatial control 3D and 4D printing, *Nat. Commun.* 2019, 10, 791.
11. G.C. Dumitrescu, I.A. Tanase, 3D Printing – A New Industrial Revolution, Knowl. Horizons. Econ. 8 (2016) 32–39. https://econpapers.repec.org/article/kh ejournl/v_3a8_3ay_3a2016_3ai_3a1_3ap_3a32-39.htm.
12. T. Pereira, J.V. Kennedy, J. Potgieter, A comparison of traditional manufacturing vs additive manufacturing, the best method for the job, Procedia Manuf 30 (2019) 11–18, https://doi.org/10.1016/j.promfg.2019.02.003.
13. N.Z. Nkomo, A review of 4D printing technology and future trends, National University of Science and Technology, Zimbabwe, 2018. https://www.researchgate.net/publication/328162917%0AA.
14. X. Li, J. Shang, Z. Wang, Intelligent materials: A review of applications in 4D printing, Assem. Autom. 37 (2017) 170–185, https://doi.org/10.1108/AA-11- 2015-093.
15. S. Tibbits, C. McKnelly, C. Olguin, D. Dikovsky, S. Hirsch, 4D printing and universal transformation, ACADIA 2014 - Des. Agency Proc. 34th Annu. Conf. Assoc. Comput. Aided Des. Archit, 2014-Octob (2014) 539–548.
16. F. Momeni, S. M.Mehdi Hassani.N, X. Liu, J. Ni, A review of 4D printing, Mater. Des. 122 (2017) 42–79, https://doi.org/10.1016/j.matdes.2017.02.068.
17. Nor Amira Izzati Ayob , Nurul Fazita Mohammad Rawi, Azniwati Abd Aziz, Baharin Azahari and Mohamad Haafiz Mohamad Kassim. "The properties of 3D printed poly (lactic acid) (PLA)/poly (butylene-adipate-terephthalate) (PBAT) blend and oil palm empty fruit bunch (EFB) reinforced PLA/PBAT composites used in fused deposition modelling (FDM) 3D printing" *Physical Sciences Reviews*, vol. 8, no. 12, 2023, pp. 5135-5151. https://doi.org/10.1515/psr-2022-0048
18. Cardoso, PHM, Coutinho, RRTP, Drummond, FR, da Conceição, MdoN, Thiré, RMdaSM. Evaluation of printing parameters on porosity and mechanical properties of 3D printed PLA/PBAT blend parts. *Macromol Symp* 2020;394:1–12. https://doi.org/10.1002/masy.202000157.
19. Liu, Z, Wang, Y, Wu, B, Cui, C, Guo, Y, Yan, C. A critical review of fused deposition modeling 3D printing technology in manufacturing polylactic acid parts. *Int J Adv Manuf Technol* 2019;102:2877–89. https://doi.org/10.1007/s00170-019-03332-x
20. Iwata, T. Biodegradable and bio-based polymers: future prospects of eco-friendly plastics. *Angew Chem Int Ed* 2015;54:3210–5. https://doi.org/10.1002/anie.201410770.Search in Google ScholarPubMed
21. Farah, S, Anderson, DG, Langer, R. Physical and mechanical properties of PLA, and their functions in widespread applications — a comprehensive review. *Adv Drug Deliv Rev* 2016;107:367–92. https://doi.org/10.1016/j.addr.2016.06.012.
22. [80] A. Pappu, K.L. Pickering, V.K. Thakur, Manufacturing and characterization of sustainable hybrid composites using sisal and hemp fibres as reinforcement of poly (lactic acid) via injection moulding, Ind. Crops Prod. 137 (2019) 260–269, https://doi.org/10.1016/j.indcrop.2019.05.040.
23. A.V. Wijk, I.V. Wijk, 3D printing with biomaterials: Towards a sustainable and circular economy, IOS Press, 2015, https://doi.org/10.3233/978-1-61499-486-2- i.

24. S.P. Dubey, V.K. Thakur, S. Krishnaswamy, H.A. Abhyankar, V. Marchante, J. L. Brighton, Progress in environmental-friendly polymer nanocomposite material from PLA: Synthesis, processing and applications, Vacuum 146 (2017) 655–663, https://doi.org/10.1016/j.vacuum.2017.07.009.
25. S. Wickramasinghe, T. Do, P. Tran, FDM-Based 3D printing of polymer and associated composite: A review on mechanical properties, defects and treatments, Polymers (Basel) 12 (2020) 1–42, https://doi.org/10.3390/polym12071529.
26. T. Mukherjee, N. Kao, PLA Based Biopolymer Reinforced with Natural Fibre: A Review, J. Polym. Environ. 19 (2011) 714–725, https://doi.org/10.1007/ s10924-011-0320-6.
27. M. Murariu, P. Dubois, PLA composites, From production to properties, Adv. Drug Deliv. Rev. 107 (2016) 17–46, https://doi.org/10.1016/j.addr.2016.04.003.
28. A.S. Getme, B. Patel, A review: Bio-fiber's as reinforcement in composites of polylactic acid (PLA), Mater. Today Proc 26 (2019) 2116–2122, https://doi.org/ 10.1016/j.matpr.2020.02.457.
29. X. Wu, W.M. Huang, Y. Zhao, Z. Ding, C. Tang, J. Zhang, Mechanisms of the shape memory effect in polymeric materials, Polymers, 5 (2013) 1169–1202, https://doi.org/10.3390/polym5041169.
30. J. Zhou, S. Sheiko, Reversible shape-shifting in polymeric materials, J. Polym. Sci. Part B Polym. Phys. 54 (2016), https://doi.org/10.1002/polb.24014 n/a-n/a.
31. S.K. Leist, D. Gao, R. Chiou, J. Zhou, Investigating the shape memory properties of 4D printed polylactic acid (PLA) and the concept of 4D printing onto nylon fabrics for the creation of smart textiles, Virtual Phys. Prototyp. 12 (2017) 290–300, https://doi.org/10.1080/17452759.2017.1341815.
32. C. Yang, B. Wang, D. Li, X. Tian, Modelling and characterisation for the responsive performance of CF/PLA and CF/PEEK smart materials fabricated by 4D printing, Virtual Phys. Prototyp. 12 (2017) 69–76, https://doi.org/10.1080/ 17452759.2016.1265992.
33. .K. Dogan, S. Boyacioglu, M. Kodal, O. Gokce, G. Ozkoc, Thermally induced shape memory behavior, enzymatic degradation and biocompatibility of PLA/ TPU blends: "Effects of compatibilization, J. Mech. Behav. Biomed. Mater. 71 (2017) 349–361, https://doi.org/10.1016/j.jmbbm.2017.04.001.
34. F.S. Senatov, K.V. Niaza, M.Y. Zadorozhnyy, A.V. Maksimkin, S.D. Kaloshkin, Y. Z. Estrin, Mechanical properties and shape memory effect of 3D-printed PLA- based porous scaffolds, J. Mech. Behav. Biomed. Mater. 57 (2016) 139–148, https://doi.org/10.1016/j.jmbbm.2015.11.036.
35. Mohapatra, AK, Mohanty, S, Nayak, SK. Study of thermo-mechanical and morphological behaviour of biodegradable PLA/PBAT/layered silicate blend nanocomposites. *J Polym Environ* 2014;22:398–408. https://doi.org/10.1007/s10924-014-0639-x.
36. Tsuji H, Ikada YJ, Blends of aliphatic polyesters. II. Hydrolysis of solution-cast blends from poly(L-lactide) and poly(E-caprolactone) in phosphate-buffered solution, (1998) J Appl Polym Sci, 67, 405–415, https://doi.org/10.1002/(SICI)1097-4628(19980118)67:3<405::AID-APP3>3.0.CO;2-Q
37. Perego G, Cella GD, Bastioli C, Effect of molecular weight and crystallinity on poly(lactic acid) mechanical properties, (1996) J Appl Polym Sci, 59, 37–43, https://doi.org/10.1002/(SICI)1097-4628(19960103)59:1<37::AID-APP6>3.0.CO;2-N
38. Bledzki A, Fabrycy E, Degradable polymers - a technical report (1992), Polimery 37, 343-350, https://doi.org/10.14314/polimery.1992.343
39. Garlotta D, A Literature Review of Poly(Lactic Acid, (2001) J Polym Env, 9, 63–84, https://doi.org/10.1023/A:1020200822435
40. T. Hamieh, New Progress on London Dispersive Energy, Polar Surface Interactions, and Lewis's Acid–Base Properties of Solid Surfaces, Molecules 29 (5), 949, https://doi.org/10.3390/molecules29050949
41. T. Hamieh, London Dispersive and Lewis Acid-Base Surface Energy of 2D Single-Crystalline and Polycrystalline Covalent Organic Frameworks, *Crystals* 2024, *14*(2), 148; https://doi.org/10.3390/cryst14020148
42. T. Hamieh, Inverse Gas Chromatography to Characterize the Surface Properties of Solid Materials, *Chem. Mater.* 2024, 2024, https://doi.org/10.1021/acs.chemmater.3c03091
43. Hamieh, T. Study of the temperature effect on the surface area of model organic molecules, the dispersive surface energy and the surface properties of solids by inverse gas chromatography. *J. Chromatogr. A* **2020**, *1627*, 461372. https://doi.org/10.1016/j.chroma.2020.461372.
44. Hamieh, T. New Methodology to Study the Dispersive Component of the Surface Energy and Acid–Base Properties of Silica Particles by Inverse Gas Chromatography at Infinite Dilution. *J. Chromatogr. Sci.* **2021**, *60*, 126–142. https://doi.org/10.1093/chromsci/bmab066.
45. Hamieh, T. New physicochemical methodology for the determination of the surface thermodynamic properties of solid particles. *Appliedchem* **2023**, *3*, 229–255. https://doi.org/10.3390/appliedchem3020015.
46. Hamieh, T.; Ahmad, A.A.; Roques-Carmes, T.; Toufaily, J. New approach to determine the surface and interface thermodynamic properties of H-β-zeolite/rhodium catalysts by inverse gas chromatography at infinite dilution. *Sci. Rep.* **2020**, *10*, 20894. https://doi.org/10.1038/s41598-020-78071-1.
47. London, F. The general theory of molecular forces. *Trans. Faraday Soc.* **1937**, *33*, 8–26. https://doi.org/10.1039/tf937330008b.

48. Saint-Flour, C.; Papirer, E. Gas-solid chromatography. A method of measuring surface free energy characteristics of short carbon fibers. 1. Through adsorption isotherms. *Ind. Eng. Chem. Prod. Res. Dev.* **1982**, *21*, 337–341. https://doi.org/10.1021/i300006a029.
49. Saint-Flour, C.; Papirer, E. Gas-solid chromatography: Method of measuring surface free energy characteristics of short fibers. 2. Through retention volumes measured near zero surface coverage. *Ind. Eng. Chem. Prod. Res. Dev.* **1982**, *21*, 666–669. https://doi.org/10.1021/i300008a031.
50. Saint-Flour, C.; Papirer, E. Gas-solid chromatography: A quick method of estimating surface free energy variations induced by the treatment of short glass fibers. *J. Colloid Interface Sci.* **1983**, *91*, 69–75. https://doi.org/10.1016/0021-9797(83)90314-4.
51. Schultz, J.; Lavielle, L.; Martin, C. The role of the interface in carbon fibre-epoxy composites. *J. Adhes.* **1987**, *23*, 45–60. https://doi.org/10.1080/00218468708080469.
52. Donnet, J.-B.; Park, S.; Balard, H. Evaluation of specific interactions of solid surfaces by inverse gas chromatography. *Chromatographia* **1991**, *31*, 434–440. https://doi.org/10.1007/bf02262385.
53. Brendlé, E.E.; Papirer, E. A new topological index for molecular probes used in inverse gas chromatography for the surface nanorugosity evaluation, 2. Application for the Evaluation of the Solid Surface Specific Interaction Potential. *J. Colloid Interface Sci.* **1997**, *194*, 217–224.
54. Brendlé, E.E.; Papirer, E. A new topological index for molecular probes used in inverse gas chromatography for the surface nanorugosity evaluation, 1. Method of Evaluation. *J. Colloid Interface Sci.* **1997**, *194*, 207–216. https://doi.org/10.1006/jcis.1997.5104.
55. Sawyer, D.T.; Brookman, D.J. Thermodynamically based gas chromatographic retention index for organic molecules using salt-modified aluminas and porous silica beads. *Anal. Chem.* **1968**, *40*, 1847–1850. https://doi.org/10.1021/ac60268a015.
56. Chehimi, M.M.; Pigois-Landureau, E. Determination of acid–base properties of solid materials by inverse gas chromatography at infinite dilution. A novel empirical method based on the dispersive contribution to the heat of vaporization of probes. *J. Mater. Chem.* **1994**, *4*, 741–745.
57. Donnet, J.-B.; Ridaoui, H.; Balard, H.; Barthel, H.; Gottschalk-Gaudig, T. Evolution of the surface polar character of pyrogenic silicas, with their grafting ratios by dimethylchlorosilane, studied by microcalorimetry. *J. Colloid Interface Sci.* **2008**, *325*, 101–106. https://doi.org/10.1016/j.jcis.2008.05.025.
58. Jagiełło, J.; Ligner, G.; Papirer, E. Characterization of silicas by inverse gas chromatography at finite concentration: Determination of the adsorption energy distribution function. *J. Colloid Interface Sci.* **1990**, *137*, 128–136. https://doi.org/10.1016/0021-9797(90)90049-t.
59. Rückriem, M.; Inayat, A.; Enke, D.; Gläser, R.; Einicke, W.-D.; Rockmann, R. Inverse gas chromatography for determining the dispersive surface energy of porous silica. *Colloids Surfaces A Physicochem. Eng. Asp.* **2010**, *357*, 21–26. https://doi.org/10.1016/j.colsurfa.2009.12.001.
60. Bauer, F.; Meyer, R.; Czihal, S.; Bertmer, M.; Decker, U.; Naumov, S.; Uhlig, H.; Steinhart, M.; Enke, D. Functionalization of porous siliceous materials, Part 2: Surface characterization by inverse gas chromatography. *J. Chromatogr. A* **2019**, *1603*, 297–310. https://doi.org/10.1016/j.chroma.2019.06.031.
61. Hamieh, T.; Schultz, J. New approach to characterise physicochemical properties of solid substrates by inverse gas chromatography at infinite dilution. *J. Chromatogr. A.* **2002**, 969(1-2), 17-47, https://doi.org/10.1016/S0021-9673(02)00368-0.
62. Gutmann, V. *The Donor-Acceptor Approach to Molecular Interactions*; Plenum: New York, NY, USA, 1978.
63. Riddle, F.L.; Fowkes, F.M. Spectral shifts in acid-base chemistry. Van der Waals contributions to acceptor numbers, Spectral shifts in acid-base chemistry. 1. van der Waals contributions to acceptor numbers. *J. Am. Chem. Soc*. **1990**, *112*, 3259–3264. https://doi.org/10.1021/ja00165a001.
64. Hamieh, T.; Rageul-Lescouet, M.; Nardin, M.; Haidara, H.; Schultz, J. Study of acid-base interactions between some metallic oxides and model organic molecules. *Colloids Surfaces A Physicochem. Eng. Asp.* **1997**, *125*, 155–161. https://doi.org/10.1016/s0927-7757(96)03855-1.
65. Hamieh, T.; Schultz, J. Study of the adsorption of n-alkanes on polyethylene surface—State equations, molecule areas and covered surface fraction. *Comptes Rendus L'acad. Sci. Sér. IIb* **1996**, *323*, 281–289.
66. Lide, D.R. (Ed.) *CRC Handbook of Chemistry and Physics*, 87th ed.; Internet Version 2007; Taylor and Francis: Boca Raton, FL, USA, 2007. http:/www.hbcpnetbase.com (accessed on 1 November 2023).
67. Van Oss, C.J.; Good, R.J.; Chaudhury, M.K. Additive and nonadditive surface tension components and the interpretation of contact angles. *Langmuir* **1988**, *4*, 884–891. https://doi.org/10.1021/la00082a018.